Environmental Technology & Innovation 41 (2026) 104708

Contents lists available at ScienceDirect

Environmental Technology & Innovation

journal homepage: www.elsevier.com/locate/eti

The synergistic performance of redox couples enhanced with phase inter-grown ceria-zirconia-alumina mixed oxides: A robust three-way catalyst for diesel exhaust abatement

Varuna Jayachandran [a], Priyadharsini Natesan [b], Balaji Chettiannan [a], Jet-Chau Wen [c], Talat Ali [d], Mohd Shkir [e,f], Elango Muniappan [a,*], Sambasivam Sangaraju [g,*]

[a] Department of Physics, PSG College of Arts & Science, Coimbatore 641014, India
[b] Department of Physics, Dr.NGP Institute of Technology, Coimbatore 641048, India
[c] Research Centre for Soil & Water Resources and Natural Disaster Prevention (SWAN), National Yunlin University of Science and Technology, Douliu, Yunlin 64002, Taiwan
[d] Department of Basic Medical Sciences, King Khalid University, PB 960, Abha 61421, Saudi Arabia
[e] Department of Physics, College of Science, King Khalid University, PO BOX 960, AlQura'a, Abha 61421, Saudi Arabia
[f] Smart Nano-Materials for Energy and Optoelectronic Devices Lab, Central Labs, King Khalid University, PO BOX 960, AlQura'a, Abha, 61421, Saudi Arabia
[g] National Water and Energy Center, United Arab Emirates University, Al Ain 15551, UAE

ARTICLE INFO

Keywords:
CeO_2-ZrO_2/Al_2O_3
Rare earths
XPS
AVL Digas analyzer
Diesel exhaust treatment

ABSTRACT

The CeO_2-ZrO_2 and Al_2O_3 (75 wt% and 25 wt%) were prepared by co-precipitation route, calcined at 500 °C for 5 h and mechanically mixed. Three compositions of Ce/Zr (20:80, 50:50, and 80:20) were synthesized and their microstructural properties was observed via X-ray diffraction (XRD), and Raman analysis. The CeO_2-ZrO_2/Al_2O_3 (Ce/Zr-50:50) sample reveals the mixed phase formation of cubic and tetragonal, which facilitates the catalytic activity via oxygen ion diffusion from O^{2-} sub-lattice to the sample surface. The CeO_2-ZrO_2/Al_2O_3 (Ce/Zr-50:50) was further investigated using High-resolution transmission electron microscope (HRTEM), Brunauer-Emmett-Teller (BET) study, X-ray photoelectron spectroscopy (XPS), and Scanning electron microscope (SEM). The surface area of CeO_2-ZrO_2/Al_2O_3 (Ce/Zr −50:50) was 91.2 m^2 g^{-1}, which provides surface active oxygen species to participate in diesel exhaust treatment via redox reactions. The XPS spectra of CeO_2-ZrO_2/Al_2O_3 (Ce/Zr −50:50) sample confirms the Ce^{3+} reduction along with the formation of oxygen vacancies. To perform catalytic reaction, the CeO_2-ZrO_2/Al_2O_3 (Ce/Zr −50:50) sample was coated on the perforated stainless-steel substrates by a unique and cost-effective technique, which could be economically advantageous to produce the catalyst for commercial uses on a large scale. The sample was tested at different load conditions. At maximum load condition, the sample exhibited substantial reduction in CO, HC, CO_2, NO_x, and smoke.

* Corresponding authors.
E-mail addresses: elango@psgcas.ac.in (E. Muniappan), s_sambasivam@uaeu.ac.ae (S. Sangaraju).

https://doi.org/10.1016/j.eti.2025.104708
Received 1 August 2025; Received in revised form 14 December 2025; Accepted 16 December 2025
Available online 17 December 2025

1. Introduction

One of the most formidable challenges for intergenerational health security, and sustainable development, especially in actively urbanizing countries like India is air pollution. The urban centers all over the world are more intricate and susceptible to air pollution. The primary factors responsible for air pollution are essential augmentation of industrial and automobile populations, uncontrolled land expansion, poor solid-waste management, and intensive greenhouse gas emissions. In association with this, poor air quality exposes the individuals to health risks such as stroke, cardio-vascular problems, stress, and anxiety (Choudhary and Gokhale, 2019; Pandey et al., 2021; Balakrishnan and Tsaneva, 2021). Exhaust from diesel engines and generator sets due to the incomplete combustion is harmful to both living beings and environment. In India, more stringent regulations of emission standard namely Bharat stage VI norms were introduced to diminish the air pollution as one-third of air pollution caused by automobiles (Khodkee et al., 2021). Many scientists and engineers adopted several techniques namely, exhaust gas recirculation (EGR), catalytic converters, electric-powered vehicles, bio-fuel to reduce pollution from automobiles. Among them, three-way catalytic converters (TWCs) have commendably mitigated and suppressed the automotive emissions to considerable extent. Ceria has been used as catalyst support oxide as they possess the oxygen storage and release capacity with the help of Ce^{4+}/Ce^{3+} redox couples (Kim et al., 2009). It is essential to emphasize that ceria consistently discloses a superior catalytic activity attributable to its strong inherent redox characteristics and reliable lattice oxygen. The enhanced redox characteristics of ceria due to its transition between Ce^{4+} and Ce^{3+} oxidation states generate the significant number of surface defects (oxygen vacancies). Despite its redox nature, properties of ceria can be modified by tailoring the size and shape. Moreover, combing the ceria with transition metals promote the catalytic activity from metal-support interactions due to its synergistic performance. Thus, ceria and ceria-related materials were extensively used in TWC for automobile pollution management over the past few decades, namely, CeO_2 and its solid solutions of transition metal doped form. Due to the reduced ionic radii of transition metals and formation of redox couples, the production of these solid solutions with CeO_2 may result in an increased catalytic performance of these materials. CeO_2 has been doped with a wide variety of transition metals namely, Fe, Mn, Co, Cu, Cr, and Ni. This led to an increase in reducibility of doped CeO_2 as ionic radius decreased. To put it in a nutshell, catalytic behavior is not only related to the redox couples but also its ionic radius (Machida et al., 2015; Fu et al., 2010; Gupta et al., 2010; Myung et al., 2015; Zhao et al., 2020). The CeO_2-ZrO_2 solid solution was the most recognized material in the automobile industry. The bulk oxygen in CeO_2-ZrO_2 solid solution actively involves redox reactions whereas in CeO_2 the process is restricted only to the sample surface. The addition of zirconium with ceria paves the most effective way for ceria stabilization. The bond distance between cerium and oxygen (Ce-O) will increase when larger Ce cations are substituted by smaller Zr cations, making the oxygen more mobile (Kanazawa et al., 2003). Earlier reports suggest that ceria-zirconia solid solution holds enhanced redox behavior, oxygen storage capacity, thermal resistance, and catalytic performance even at low temperatures. These properties are the result of structural imperfections obtained from the Zr^{4+} inclusion into ceria lattice, which distorts the O^{2-} sub-lattice, where reduction extends to bulk. The composition of the Ce/Zr impacts low temperature reducibility. At low Zr-content, the catalyst support is of Ce-rich in cubic symmetry, whereas at higher Zr-content, tetragonal and monoclinic phases are obtained (Petkovich et al., 2011). In the intermediate composition, mixed phases are segregated. As a result, there are no clear defined boundaries between the existences of these phases because the distortion is constantly changing with sample composition. Moreover, this distortion is sensitive to the particle size of the mixed oxides (Monte and Kašpar, 2004). The addition of alumina with an ideal content between 10 wt% and 75 wt% ratio of ceria-zirconia system provides appreciable structural, textural, and thermal stability to maintain reducing agent-to-oxidizing agent ratio close to symmetry in-order to convert the toxic pollutants to eco-friendly products (Hongmei et al., 2010). Despite the numerous advantages of alumina addition in catalyst compositions, phase segregation still arises at intermediate composition range.

The reducibility and thermal behavior of the catalyst materials not only depend upon the composition, and appropriate material usage, which also significantly influenced by the preparation techniques (Letichevsky et al., 2005). Kozlov et al., reported that the various preparation routes provide different contact of interactions between ceria and zirconia result in diverse redox properties upon calcination. Cogelled approach shows improved redox behavior than impregnation procedure, which exhibits drastic declination in homogeneity and redox characteristics (Kozlov et al., 2002). Fuentes et al., (2008) prepared three compositions of CeO_2-ZrO_2 (50, 70, 90 mol%) nanotubes via commercial polycarbonate membrane route resulting in cubic and tetragonal phase segregation (Fuentes et al., 2008). Rossignol et al., suggested that the modified sol-gel method synthesized CeO_2-ZrO_2 oxides, calcined at 600 °C, cubic phase dominates the tetragonal phase, when Ce/Zr ratio less than 0.75. While, Ce/Zr ratio is more than 0.75, only cubic phase persists (Rossignol et al., 1999a). Rossignol et al., prepared mixed phases of cubic and tetragonal ($Ce_xZr_{1-x}O_2$, $0.75 \leq x \leq 1$) by co-precipitation method, calcined at 900 °C (Rossignol et al., 1999b). Due to the exceptional thermal resistance, chemical stability, redox characteristics, and ion exchange capacity, zirconia has been extensively employed with ceria as catalyst supports, they reported (Yu et al., 2014). Even at extremely small quantity of zirconia (5 wt%) combined with ceria, improved the oxygen storage capacity (OSC) for more than 30 times were witnessed, compared to ceria alone used as catalytic material. By generating oxygen vacancies, elevation in the oxygen mobility and make more oxygen available for diesel exhaust treatment was realized (Dai et al., 2014). Thus, the catalytic actions for diesel exhaust pollutants were greatly aided by Zr, which also serves as a great stabilizer and promotes various oxygen transfers in various environments (Lee et al., 2018). The catalysts performance was further improved by alumina as stabilizer or dispersant which enhances the thermal stability by restricting the sintering of the samples. Recent research with superior performance of Ce-Zr-Al often coupled with the noble -metals like Pd and also some additional promoters such as La or P to achieve greater catalytic efficiency towards diesel exhaust pollutant treatment (Chen et al., 2022; Guo et al., 2024; Feng et al., 2024). While these research works highlights the catalytic activity of the Ce-Zr-Al oxides but they highly rely on the noble-metal supports.

After considering all the above aspects, herein we develop economic-friendly CeO_2-ZrO_2/Al_2O_3 catalyst supports, which can be produced in large scale and easy to commercialize globally. The synthesis of low-cost, noble-metal free CeO_2-ZrO_2/Al_2O_3 catalyst and

preparation of catalyst substrates are as follows. We have synthesized ceria-zirconia mixed oxides at various proportions of Ce/Zr by a simple and facile co-precipitation route. Powder form of alumina was also prepared by precipitation technique and was mechanically mixed with ceria-zirconia at 25 wt%. The structural, textural, chemical, morphological, and compositional properties of the samples were analyzed. The observed redox couples (Ce^{4+}/Ce^{3+}) and mixed phases of the CeO_2-ZrO_2/Al_2O_3 (Ce/Zr −50:50) sample acts as an oxygen buffer which, distorts the local oxygen environment inside the sample. The interfacial boundary of the mixed phases boosts the oxygen diffusion for better catalytic activity. This sample was coated on the perforated stainless-steel substrates by a novel approach preceded by proper cleaning techniques and they are kept inside the custom-made exhaust manifold. The emission analysis was done in Field Marshal diesel engine using AVL Digas analyzer. Under lean-burn conditions, the significant reduction of NOx is more challenging and it is greatly achieved by CZA-55 sample makes a potential candidate for more advanced technological developments in automobile industry.

2. Materials and methods

2.1. Chemicals

In this work, we used nitrate salts of cerium [$Ce(NO_3)_3{\cdot}6H_2O$, 99 %], zirconium [$ZrO(NO_3)_2.xH_2O$, 99 %], and aluminum [$Al(NO_3)_3{\cdot}9H_2O$, 99 %] were obtained from Sigma Aldrich. Ammonia (NH_4OH, 25 wt%) and ethanol (C_2H_5OH) were purchased from MERCK. We have used all chemicals as received without further purification.

2.2. Preparation route

CeO_2-ZrO_2/Al_2O_3 oxides were prepared via simple and facile co-precipitation approach with three different proportions of Ce/Zr (20:80, 50:50, 80:20) and mechanically mixed with fixed 25-wt% of Al_2O_3. Equal volumes of ethanol and distilled water were mixed to obtain bi-solvent, in which the nitrate salts of cerium and zirconium were mixed. The mixed solution was allowed for vigorous stirring to attain homogeneous and the complete dissolution of the precursors. The precipitating agent NH_4OH was added drop-wise into the reaction medium at room temperature. The pH of the medium was maintained at 10, where the reaction environment leads to the formation of M-OH (M= Ce, Zr). The precipitate was stirred continuously for about 7 h and aged overnight at room temperature. The obtained precipitate was centrifuged at 3000 rpm for 15 min and washed several times with distilled water and organic solvents (ethanol and acetone) in order to remove the impurities and unreacted precursors. Then, calcination was done in a muffle furnace at 500 °C for 5 h, thus the precipitates were transformed as CeO_2-ZrO_2 nanoparticles.

Al_2O_3 nanoparticles were prepared by following the aforementioned protocol and 25 wt% of prepared alumina was mechanically mixed with 75 wt% of CeO_2-ZrO_2 nanoparticles. The synthesized samples were named as CZA-28, CZA-55, and CZA-82 based on their relative Ce/Zr ratios 20:80, 50:50, and 80:20 respectively (Lan et al., 2014; Jayachandran et al., 2022).

2.3. Monolith preparation

The traditional catalytic converter (Supplementary Figure. 1) was slightly modified and made completely leak-proof with the help of gaskets. The body of the catalytic converter was a cylindrical stainless steel – 316 L (SS) pipe with a dimension of 6 in. × 4 in. × 3 mm. The inlet and outlet of the converter was also a 2-inch SS pipe with 32 mm diameter and 3 mm thick. The stainless-steel (SS) plates of 1 mm thickness were chosen as the catalyst substrates were finely cut into circular discs of 80 mm diameter with the help of LASER. The perforation was done with an angle shift of 15° for each plate to reduce exhaust back pressure. In conventional catalytic converter, the ceramic monoliths (oxidation and reduction beds) were used; we have replaced them by stacking the SS plates and separated them with a sleeve. The perforated SS substrate was washed using liquid soap in ultrasonic bath for 30 min, then using acetone for 30 min, with each stage being followed by a 2-hour drying phase at 100 °C. The substrate was also pre-heated to provide them a rough surface that would help the adherence of nano- catalyst on substrate. The substrate surface was etched with emery paper and then thoroughly cleaned with acetone and distilled water followed by drying in hot air oven at 50 °C for 30 min.

Table 1
Field Marshal engine specifications.

Engine Specifications	
Make/Model	Field Marshal. Model- TRM II No.
Engine Type	Four stroke, water-cooled
Number of Cylinders	Single
Engine Starting	By hand Cranking method
Type of fuel	Diesel
Bore diameter	114.3 mm
Stroke length	130 mm
Speed	850 rpm
Dynamometer	Eddy current dynamometer
Compression ratio	16.1
Rated power	5.9 KW

The SS substrates were coated with prepared catalyst nanoparticles via a novel technique using M-seal and araldite. Equal amounts of both the glues were mixed and applied over the perforated stainless-steel substrates. The catalyst particles were coated using thin sieve on the glued substrate surface. The present work focused to decrease the price of the conventional catalytic converters with the help of simple and cost-effective coating technique. The substrates were inserted inside the designed catalytic converter and then attached to the exhaust manifold of the diesel engine for emission analysis (Jayachandran et al., 2022). Table 1 specifies the design of the Field Marshal diesel engine.

The substrates were stacked in an order and separated by SS sleeves. The modified catalytic converter was completely sealed with rubber gasket and bolts to make them leak-proof. The time period of the emission test for each load condition took nearly 2–2.5 h. The outer-body temperature of catalytic converter was approximately 250 ℃.

The determination of t-plot for BET analysis is evaluated by using the relation (Choudhary and Gokhale, 2019)

$$t \quad (angstrom) = \{ \quad \frac{13.99}{\log\left(\frac{P_0}{P}\right) + 0.034} \quad \}^{\frac{1}{2}} \tag{1}$$

The Ce^{3+} concentration from XPS analysis was calculated from the formula (Pandey et al., 2021)

$$Ce^{3+}(\%) = \frac{Ce^{3+}}{Area\ of(Ce^{3+} + \quad Ce^{4+})} \quad \times 100\% \tag{2}$$

3. Sample characterization

The microstructural properties and phase purity were examined using an X'Pert Pro diffractometer with a Cu K_α (1.5406 Å) source. Raman spectral investigation made with BRUKER RFS 27 Standalone FT-RAMAN spectrometer revealed the additional structural information and phase analysis of CZA samples. The HRTEM facility was used to collect topography, 3D morphology, and lattice orientations employing a Japan-made JEOL-JEM (2010) microscope. The HRTEM system comprises with BRUCKER QUANTAX 200-Z10 EDX detector, which helped to determine the elemental composition of the prepared CZA samples. The N_2- physisorption principle at 77 K with a saturated vapor pressure of roughly 96.582 KPa, BELSORP Mini II was used to determine the surface area, pore diameter, and pore volume. Surface analysis of the samples was performed using a surface-sensitive X-ray photoelectron spectrometer (XPS), a Versa Probe-III (Physical Electronics) enabled with Al-K_α of energy 1486.6 eV operated at 400 W. The surface morphology was examined using a TESCAN MIRA-3 Scanning Electron Microscope (SEM) along with an EDAX detector. The mechanical properties of the coated substrates were studied using nano-indentation test conducted via Berkovich diamond tip. The catalytic activity was scrutinized using stationary Field Marshal diesel engine along with AVL Digas analyzer.

4. Results and discussion

4.1. X-ray diffraction analysis

The microstructural properties and phase purity of prepared CZA-28, CZA-55, and CZA-82 were examined. The X-ray diffractogram for the above examination was depicted in Fig. 1. It clearly evidenced the microstructural assessment of the prepared ceria-zirconia-alumina (CeO2-ZrO2/Al2O3) complex systems. The composition and calcination temperature have a considerable impact on the observed reflections of the samples. The non-existence of alumina peak in XRD evidences the homogeneously dispersed state of alumina inside the CeO_2-ZrO_2 lattice (Wei et al., 2008). The CZA-28 sample shows ZrO_2-rich tetragonal phase signifies low cerium

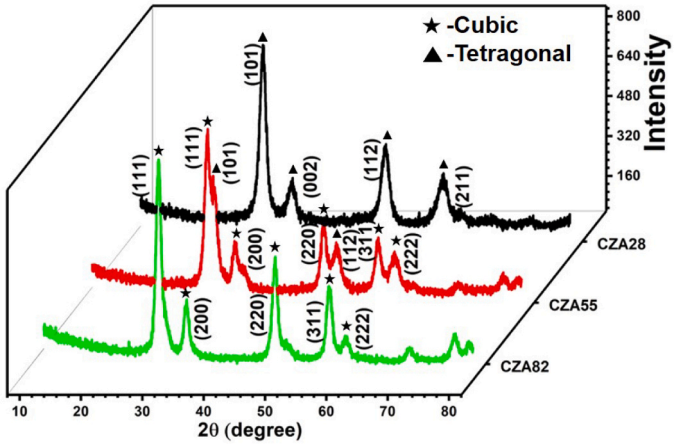

Fig. 1. X-ray diffractogram of CeO_2-ZrO_2/Al_2O_3 mixed oxides.

content ≤ 20 wt% at 2θ = 30.1° (101) with space group *P4$_2$/nmc* (ICDD: 80–0785). The observation of stable single tetragonal phase for addition of 20 wt% of CeO_2 shows zero other phase segregation but with the slight shift in 2θ towards higher trend. The CZA-55 exhibits the mixed phases of cubic and tetragonal with dominance of the cubic symmetry at 2θ = 28.7° (111). When Ce/Zr ratio is 1, the ceria (111) and zirconia (101) peaks overlap and appear as doublets with peak broadening at 2θ = 28.7° to 30.3°. Sylvie Rossignol et al., (Rossignol et al., 1999b) reported that CeO_2-ZrO_2 prepared via co-precipitation approach yields the mixed phases of cubic and tetragonal, whereas the sol-gel technique derived the solid-solution. Idriss Atribak et al., (Atribak et al., 2009) presented that the segregation of cubic and tetragonal phases of the sample prepared by physical mixtures of nitrate salts using Ash-free carbon fiber template. The CZA-82 sample depicts the CeO_2-rich cubic fluorite crystal structure holds high ceria content ≥ 80 wt%) with space group F*m*-3*m* (ICDD: 34–0394) at 2θ = 28.6°. XRD patterns of our samples reveal the tetragonal, cubic with tetragonal and cubic phase alone for the samples CZA-28, CZA-55, and CZA-82, respectively. Table 2 provides the microstructural information of the prepared samples.

The inclusion of Zr^{4+} ions inside the structural framework of the CZA-28 and CZA-82 samples witness the absence of phase separation indicating the solid solution formation. The Ce^{4+} (0.097 nm) ion reduced to Ce^{3+} (0.107 nm) ion due to the existence of smaller Zr^{4+} (0.084 nm) ion, resulting in cubic cell contraction (from 0.544 nm (bulk) to 5.2440 nm). The cubic cell parameter declined due to the introduction of Zr^{4+} ions into ceria lattice (Fornasiero et al., 1996). In CZA-55 sample, the suppression of peak intensity and peak broadening provides the greater full-width half maxima (FWHM), which contributes the particle size reduction compared to CZA-28 and CZA-82 (Fu et al., 2009). The multi-faceted nanoparticles of CZA-55 display aggregation to lower extent and are discussed in TEM analysis. The cubic and tetragonal phases of the CZA-55 sample show a substantial synergetic impact at the catalyst interfaces. It further provides an intriguing pathway to enhance the electronic structure of the anions. This promotes catalytic performance by ensuring the sufficient mobility of oxygen ions from the O^{2-} sub lattice to the surface (Jayachandran et al., 2022; Zhou et al., 2021). Thus, the smaller sized CZA-55 particles improve the redox nature of the samples, which initiates the Mars-Van-Krevelen mechanism by involving the surface oxygen vacancies in order to eliminate the toxic elements of the diesel engine.

4.2. Raman analysis

Raman spectra investigation reveals additional structural information and phase analysis of CZA samples. The Raman spectra (Fig. 2) of CeO_2-ZrO_2 oxides show tetragonal phase with characteristic bands of zirconia when it is ≥ 20 wt%. The tetragonal phase originates from the six Raman active modes as bands namely $A_{1g} + 3E_g + 2B_{1g}$ located at 142, 258, 311, and 622 cm^{-1} (Li et al., 2016). These bands correspond to the t" phase (t-ZrO_2, space group *P4$_2$/nmc*) along with a Raman band at 466 cm^{-1}, attributed to cubic symmetry Raman active mode (F_{2g}) of CeO_2. The presence of this cubic phase is reasoned for the reduction of Ce^{4+} ion as Ce^{3+} ion with the generation of oxygen vacancies. The CZA-55 sample (Fig. 2**c**) shows the high intense F_{2g} Raman band at 465 cm^{-1} assigned as triply degenerated symmetric stretching vibration mode of Ce-O bond. The broad band at 259–302 cm^{-1} denotes the overlapped band of t-phase of ZrO_2 retain the cubic cation sub-lattice whereas the oxygen atoms undergo the tetragonal deformation (Zhao et al., 2010). The t" phase is commonly known as extended cubic phase. The cations in the cubic c and t" phase occupies the same positions whereas; the oxygen ions undergo tetragonal distortions. It is practically impossible to distinguish t" phase and cubic phase using XRD as it is insensitive to light elements like oxygen along with the presence of heavy element such as cerium (Zhang et al., 2006). Only Raman spectra can identify the metastable t" phase, since diffraction ability of anion atoms was limited in XRD.

The incomplete phase transition from cubic to tetragonal depends upon the zirconia content. A low intense band at 608 cm^{-1} arises due to the relaxation of symmetry caused by the movement of oxygen from its lattice point to the new interstitial position. This creates two types of defects in native crystal namely interstitial and point defects (Piumetti et al., 2016). The tetragonal distortion moves the oxygen ions to octahedral sites by elongating the metal-oxygen bonds, which creates an interesting pathway to conduct oxygen ions by lowering the energy barrier (Kuhn et al., 2013). The Frenkel-type anion defects present in the nano-dimensional oxides facilitate the catalytic performance. In CZA-82 sample, the F_{2g} Raman active band shifts to lower wavelengths (465 cm^{-1}) for the sample with ceria content ≥ 80 wt%. The origination of band at 311 cm^{-1} is attributed to oxygen ion displacement due to the partial breakdown of *Fm3m* crystal symmetry. Zr^{4+} ion insertion into the CeO_2 lattice creates a considerable number of oxygen vacancies that results in the evolution of weak band at 618 cm^{-1} in Raman spectra. The dearth of fundamental peaks of alumina is also observed, which is in consistent with XRD findings.

Table 2
Microstructural properties of CZA-55.

Sample Compositions	Miller planes	Crystallite size (nm)[a]	Lattice parameter (Å)[a]	Lattice strain (ε)[a]	Position of Raman active band F_{2g} (cm^{-1})[b]
CZA-28	(101)	18	a=b= 3.6101 c= 5.1832	3.11×10^{-3}	466.76
CZA-55	(111) (101)	15	a=b= 3.6131 c= 5.2440 a=b=c= 5.38239	2.818×10^{-3}	465.30
CZA-82	(111)	19	a=b=c= 5.3955	3.109×10^{-3}	465.30

[a] determined by XRD analysis.
[b] determined by RAMAN spectroscopy.

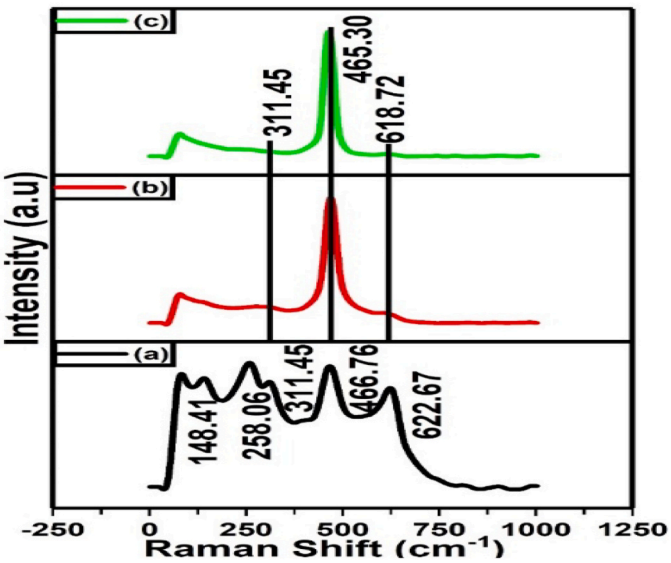

Fig. 2. Raman spectra of CeO_2-ZrO_2/Al_2O_3 mixed oxides, **(a)** CZA-28, **(b)** CZA-55, and **(c)** CZA-82.

4.3. High resolution-transmission electron microscope (HR-TEM) analysis

The HRTEM along with EDAX facility was used to collect information such as topography, 3D morphology, lattice orientations and, elemental composition of the prepared CZA sample. Fig. 3(a-c) displays the HR-TEM micrographs of the sample with 1:1 ratio of Ce/Zr, this catalyst reveals the mesoporous worm-like structures, which were discussed later in BET adsorption study (Chen et al., 2011). The addition of alumina nanoparticles through mechanical mixing method is well dispersed with strong interaction with CeO_2-ZrO_2 oxides in phylloid formation (Papavasiliou et al., 2009). The obtained clear lattice fringes in HR-TEM halos of the examined sample suggest that the nanoparticles are in well crystalline order. Fig. 3d illustrates the premeditated lattice fringes from the GATAN software depict the interplanar spacing of the lattice to be 0.29 nm corresponding to miller plane (111) of the predominant cubic phase of CZA-55 (Yang et al., 2014). The SAED pattern of the sample exhibits the polycrystalline nature, a set of clear concentric rings further indicate the miller planes of the mixed phases of cubic and tetragonal as evidenced by XRD study. The elemental mapping shown in Fig. 3e elucidates the signals of cerium (Ce), zirconium (Zr), alumina (Al), and oxygen (O), which signifies the purity of the sample prepared. The compositional homogeneity was maintained at this calcination temperature with mixed phases, which favors the redox properties of the sample.

4.4. Brunauer-Emmett-Teller (BET) analysis

The N_2- physisorption principle at 77 K with a saturated vapor pressure of roughly 96.582 KPa, BELSORP Mini II was used to determine the surface area, pore diameter, and pore volume of the sample. The Brunauer-Emmett-Teller (BET) performs the textural examination of the sample CZA-55 as shown in the Fig. 4a. According to the IUPAC classification, the sample exhibits typical type-IV characteristics of mesoporous structures. A well-defined H2 hysteresis loop observed in a relative pressure P/P_0 at 0.98 with a sharp adsorption and desorption branch that resembles hierarchical scaffolds and wormhole-like mesostructures formed by the nanoparticle aggregates (Deng et al., 2012). The BET analysis depicts the narrow particle size distribution with mesoporous channels to promote the oxygen ion mobility to interact with the soot molecules (Venkataswamy et al., 2014). The CZA-55 sample possesses the smaller crystallites with mixed phase compositions compared to CZA-28 and CZA-82 samples.

In the intermediate CeO_2-ZrO_2 content, the internal distortion of anions takes place with deformation of cubic symmetry to metastable tetragonal phase (t''). This also provides the surface area of about 91.2 $m^2\ g^{-1}$ which is relatively high on comparing with the early reports. Many reports witness the intermediate composition range contributes the better active redox couples with appreciable structural defects to instigate the reaction to get optimum results (Aneggi et al., 2006; Enzo et al., 2000; Yashima et al., 1998). The BJH plot (Fig. 4b) of CZA-55 shows a narrow unimodal-pore size distribution curve centered at 2.14 nm with a pore volume of 0.1209 $cm^3\ g^{-1}$. The t-plot (Fig. 4c) of the sample indicates the lack of micropores from the absence of positive intercept, which eventually conveys the samples are mesoporous in nature. The t-plot was obtained from the relation given in Section 2.3 (Terribile et al., 1998).

4.5. X-ray photoelectron spectrometeric (XPS) analysis

Surface analysis of the samples was performed using surface-sensitive X-ray photoelectron spectrometer (XPS), which also say

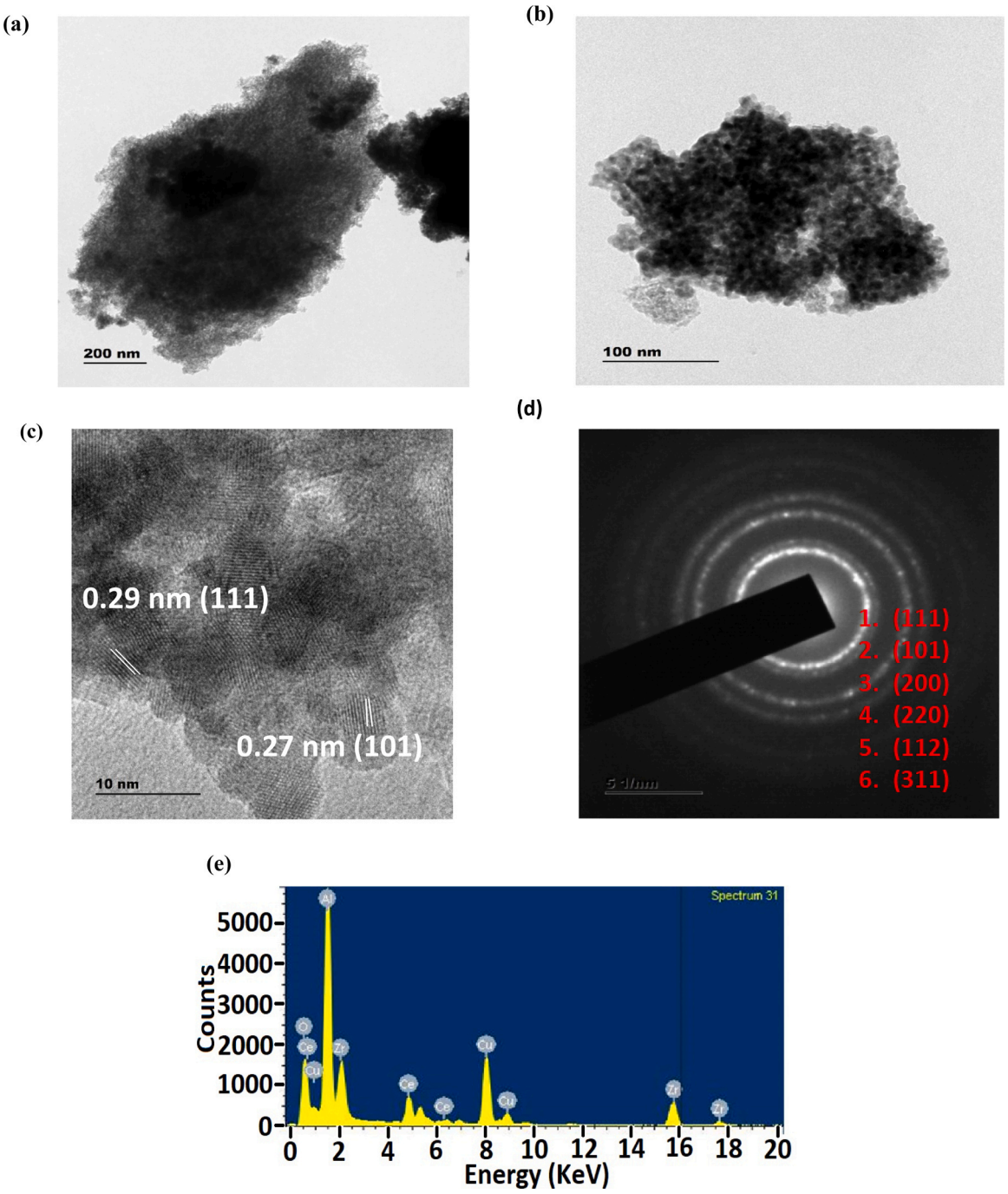

Fig. 3. **(a, b, c)** HRTEM images, **(d)** SAED pattern, and **(e)** EDS spectra of CZA-55.

about the surface chemical composition and oxidation/valence state of the elements present in the sample through examining the peak intensity and spectral line shape via XPS probe. The XPS spectra of Ce-3*d*, Zr-3*d*, Al-2*p*, and O-1*s* core levels of CZA-55 were recorded and shown in the Fig. 5**a**. Chemical analysis done by XPS was tabulated in Table 3. It is known that core-level Ce-3*d* spectra are complex to differentiate the oxidation states of CeO_2 due to the co-existence of Ce^{4+} and Ce^{3+} states. The generation of satellite peaks in Ce-3*d* profile is mainly due to the primary photoionization process occurs from the hybridization of the ligand (O-2*p*) and the metal (Ce-4*f*) and their spin-orbit coupling. The deconvolution of Ce-3*d* core level spectra (Fig. 5**b**) using Gaussian curve fitting of the peaks is labeled as per Burroughs notation (Burroughs et al., 1976). The obtained eight peaks correspond to the spin-orbit multiplets (Ce-3$d_{3/2}$ and Ce-3$d_{5/2}$) of CeO_2. The six peaks u, u", u"' and v, v", v"' are attributed to the Ce^{4+} state. The two peaks u' and v' assigned to Ce^{3+} state. The spin-orbit components u (882.9 eV) and v (900.7 eV) represents the Ce^{4+} hybridization $3d^9\ 4f^2\ O\ 2p^4$ state, whereas, the

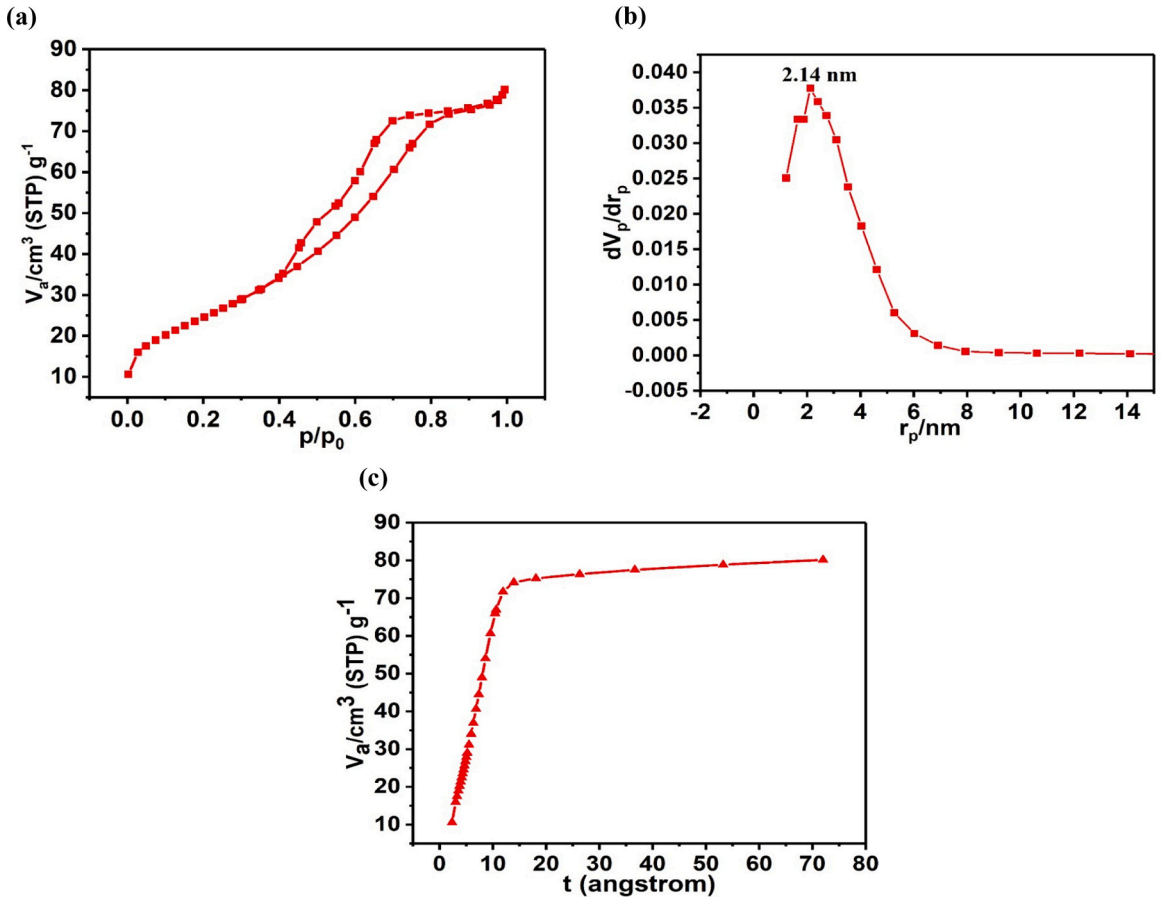

Fig. 4. **(a)** Nitrogen-sorption isotherm, **(b)** BJH plot, and **(c)** t-plot of CZA-55.

multiplets u" (889.2 eV) and v" (907.3 eV) refers to the hybridization state of Ce (IV) $3d^9\ 4f\ ^1O\ 2p^5$. These two states with lower binding energies were called as "Shake-down" satellites, in which electrons of O-2*p* transferred to Ce-4*f* (Mullins et al., 1998). The doublets u"' (898.2 eV) and v"' (916.9 eV) denotes the Ce (IV) $3d^9\ 4f^0$ O $2p^6$ hybridization state. The peaks u′ (885.9 eV) and v′ (903.7 eV) indicates the Ce (III) $3d^9\ 4f^2$ O $2p^5$ hybridization corresponds to Ce^{3+} state (Anandan and Bera, 2013). The calculated Ce^{4+} content from the peak area was 83.67 % while Ce^{3+} concentration was 16.33 %. The presence of Ce^{3+} ions from Ce^{4+} reduction confirms the non-stoichiometric nature of CeO_2 that creates the charge imbalance, unsaturated chemical bonds and oxygen vacancies. This inherent natural property of CeO_2 helps the oxygen ions to migrate from bulk to the surface for initiating the redox cycle of the catalyst (Wan et al., 2011). The relative Ce^{3+} concentration was evaluated from the relation given in the Section 2.3 and are tabulated in Table3 (Aneggi et al., 2006)

The Gaussian fitted Zr-3*d* core level spectra (Fig. 5c) reveal the spin-orbital peaks split into $3d_{5/2}$ and $3d_{3/2}$ multiplets at 182.21 eV and 184.46 eV respectively. The energy difference between spin-orbitals was around 2.2 eV, which affirms that the Zr exists in ZrO_2 form not as metallic zirconium (Galtayries et al., 1998). The peak at 185.91 is attributed to Zr(OH) it further allows us to presume that the presence of Al_2O_3 naturally a hygroscopic system induce the zirconia to attract hydroxyl molecule or due to the atmospheric contact during sample loading. The Al-2*p* core spectra (Fig. 5**d**) provide two peaks positioned at 74.63 eV (Al^{3+}) and 76.5 eV (AlO (OH)). The Al^{3+} peak ensures that exists as Al_2O_3. The peak at 76.5 eV might be due to the hygroscopic nature of alumina (Lu et al., 2017).

From the Fig. 5**e**, we have identified the binding energy of the lattice oxygen (O_2^{2-}/O^-) as 529.64 eV (O1) signifies the metal-oxygen-metal bond (M-O-M, where M = Ce, Zr, and Al) (Sellick et al., 2013). The defect oxide or low-coordination surface oxygen ions are assigned in the region of 531.75 eV (O2). The peak positioned at 533.89 eV (O3) corresponds to the -OH/H2O/carbonate species adsorbed from the ambient exposure. Atomic percentage (at%) of O2 indicates the higher oxygen vacancies which increases the mobility of defect oxides. These oxygen species strongly reliant on Zr content and reaction conditions, the intensity of the O-1*s* peak solitarily independent of their presence (Elidrissi et al., 2000). Now, the spectra indicate that the relative area of O2 peak is appreciable supporting the existence of surface-active Ce^{3+}-O_v-Zr^{4+} sites participates in the proposed Mars-van Krevelen pathway towards the diesel exhaust pollutant treatment. The catalyst activity was enhanced by presence of these oxygen species. The presence of Ce^{3+} states in the spectra eventually indicates the formation of oxygen vacancies as exhibited in Raman spectra, which support the catalytic conversion.

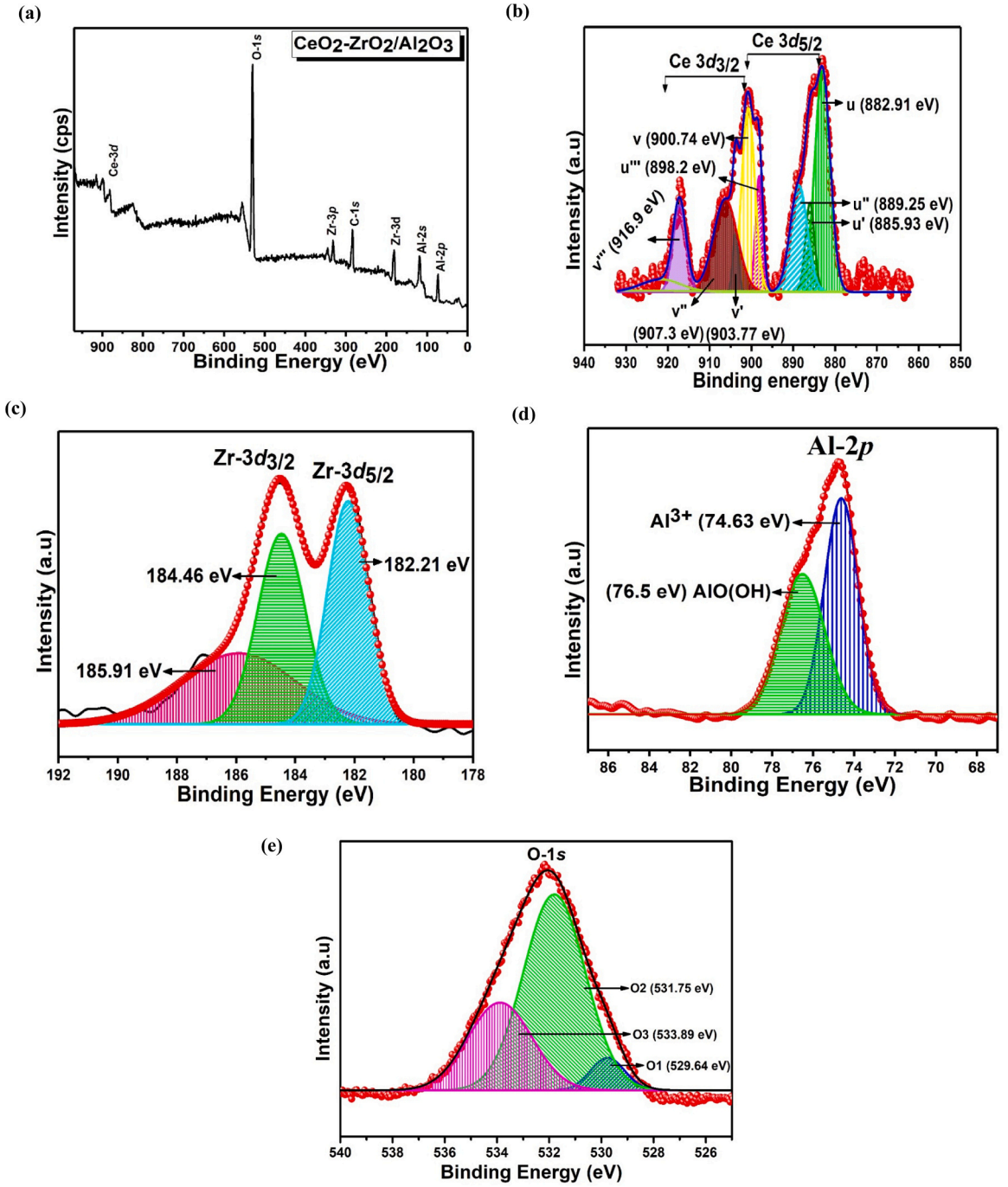

Fig. 5. (a). XPS survey spectra of CZA-55, (b) Core level spectra of Ce-3*d* (c) Zr-3*d*, (d) Al-2*p*, and (e) O-1*s*.

4.6. Scanning electron microscope (SEM) analysis

The surface morphology of CZA-55 was examined to study the morphological features and is shown in the Supplementary Figure. 2 (a-c). The SEM images depict that the sample with irregular particles formed from the trivial aggregation of smaller particles with no definite shape and are randomly orientated (Lan et al., 2014). The low agglomerated particles are in smaller in size range due to the presence of alumina particles, which helps in grain growth hindrance. The micrograph shows the mesoporous (ca. 2.12 nm) nature of the particles as described in BET investigation. The co-precipitation process enables both precipitation and aggregation of formed metal hydroxides concurrently, as well as the possibility of interplay between the precipitated nanoparticles. These nanoparticles

Table 3
Surface chemistry of CZA-55.

Sample Composition	Relative amount (%)[a]		Ce/Zr ratio[a]	Ce^{3+} (%)[a]	Defective oxygen (%)[a]	Surface area, pore diameter and pore volume.[b]
CZA-55	Ce-3d	2.36	0.89	83.67	10.14	91.2 m^2g^{-1}
	Zr-3d	2.63				2.12 nm
	Al-2p	17.62				0.1209 cm^3g^{-1}
	O-1s	50.62				
	C-1s	26.77				

[a] evaluated from XPS spectroscopy
[b] evidenced from BET analysis

interact more effectively with one another after drying the metal hydroxide to metal oxide by calcination procedure. Thus, the co-precipitation technique yields mesoporous particles with densely agglomerated morphology (Kim et al., 2009). The mesoporous materials act as oxygen promoters with eminent reducibility that allows the oxygen ion mobility from bulk to surface, where the redox mechanism happens (Ren et al., 2017).

The compositional analysis was also carried out for the prepared samples using energy dispersive spectroscopy as shown in the Supplementary Figure. 2**(d-e)**. The observation of carbon peak is due to the use of carbon tape to load the sample for analysis. The Ce, Zr, Al, and O elements are witnessed in the spectrum. Elemental composition confirms the existence of tricatalyst core elements with zero impurity peaks, which establish the contamination-free state of CZA systems.

4.7. Catalytic activity study

The prepared nano-catalyst support materials were scrutinized for three-way catalysis reactions inside the catalytic converter attached to a stationary Field Marshal diesel engine (Supplementary Figure. 1**)**. The Table 1 represents the engine specifications. From the extensive investigations on the physiochemical properties, we have decided Ce/Zr = 50:50 since we have limited resources and facilities to carry out emission analysis for all the prepared samples. From XRD, Ce/Zr = 1 ratio exhibits mixed phases of cubic and tetragonal and BET reveals the higher surface area of 91.2 $m^2\ g^{-1}$ and sufficient oxygen vacancy content from XPS corroborates the synergistic performance of Ce and Zr. The catalyst substrates of catalytic converter were made of stacked perforated SS circular discs coated with CZA-55 sample attached to the exhaust manifold of the diesel engine outlet. The engine operated at no load condition for one hour to attain the idle state. Then, the exhaust gases were analyzed using AVL gas analyzer at zero load, 25 % load, 50 % load, and 75 % load conditions. The emission control analysis was done as per the stringent regulations followed for the pollution control board in India (Dey and Mehta, 2020). The readings from AVL Digas analyzer were carefully noted for the experiment conducted without catalytic converter (CC) and with sample coated catalytic converter.

The mechanical property (Hardness and Elastic modulus) testing using a nano-indenter (Berkovich diamond tip) to study the response of coating under localized deformation. The maximum load employed was 5 mN and the indents were placed 20 μm apart. The maximum penetration depth was limited to 10 % of the coating thickness ($\leq$ 4 μm), in order to minimize the substrate influence. The data from load-hold-unload protocol, the hardness (H) and Elastic modulus (E) was evaluated using Oliver-Parr technique. The nano-indentation derived hardness and elastic modulus was presented in the supplementary Figure. 5. The average hardness of the CZA-55 coating before thermal stress was found to be H= 7.4 $\pm$ 0.8 GPa, and elastic modulus, E = 137 $\pm$ 15 GPa. After thermal treatment done at 450 ℃ for 10 h, the average hardness H= 8.5 $\pm$ 0.9 GPa, and elastic modulus E = 160 $\pm$ 22 GPa. These values indicate superior mechanical stability, as it maintains 90 % of their initial values (Before aging) even after 10 h of aging at 450 ℃. The observed data falls similar to the CeO_2-ZrO_2 materials (H=4–8 GPa, E = 90–160 GPa) (Wu and Zhang, 2013).

On the contrary, the earlier literature of CeO_2 or Ce-doped ZrO_2 coating reveals E > 200 GPa and H > 20 GPa, whereas α-Al_2O_3 coating exhibits 25 GPa of H and 400 GPa of E (Vojtko et al., 2020; Ruppi et al., 2008). The CZA-55 sample possesses porous catalytic structure for the oxygen ion mobility. The obtained H/E ratio lies between ~0.5–0.55, which indicates the coating represents a favourable balance between H and E. The coating is mechanically stable and provide an ideal surface for redox treatment with appreciable crack resistance and resilience towards thermal shock during the exhaust treatments.

The exhaust gas from the outlet of the catalytic converter was provided as feed to the AVL gas analyzer and smoke meter to note the readings and their corresponding Error bar diagram was presented in the Supplementary Figure. 3 & 4. The AVL gas analyzer shows the readings of carbon monoxide (CO), hydrocarbon (HC), carbon dioxide (CO_2), oxygen (O_2), and nitrogen oxides (NO_x) while the smoke meter indicates the quantity of smoke released from the diesel engine as given in the Fig. 6a-f. The CZA-55 sample is studied for CO oxidation, which strongly depends on surface oxygen active sites contribute in Mars-van-Krevelen mechanism (Dey and Dhal, 2020). At 75 % load condition, the CO oxidized to CO_2 more than 50 % compared to the value observed without catalyst support systems. In human body, CO gases when inhaled, it converts the hemoglobin to carboxy-hemoglobin which eventually reduces the oxygen carrying capacity in blood. The HC emission was reduced by converting them to water vapor and carbon dioxide via redox reactions carried out by the CeO_2-ZrO_2/Al_2O_3 catalyst. The HC molecules adhered to the sample surface combines with the oxygen to form H_2O and CO_2. This reaction process continues until the lattice oxygen migrates from lattice to the surface. At maximum load condition, the HC exhibits the 30 % of reduction. The NO_x emission undergoes a vigorous reduction to give harmless N_2 gas. The CO_2 and O_2 gases were also realized with the help of AVL gas sensors. The smoke meter shows the maximum reduction of 68 % at the high load condition. The exhaust gases were treated with the help of two parameters one surface active oxygen species and the other from generated

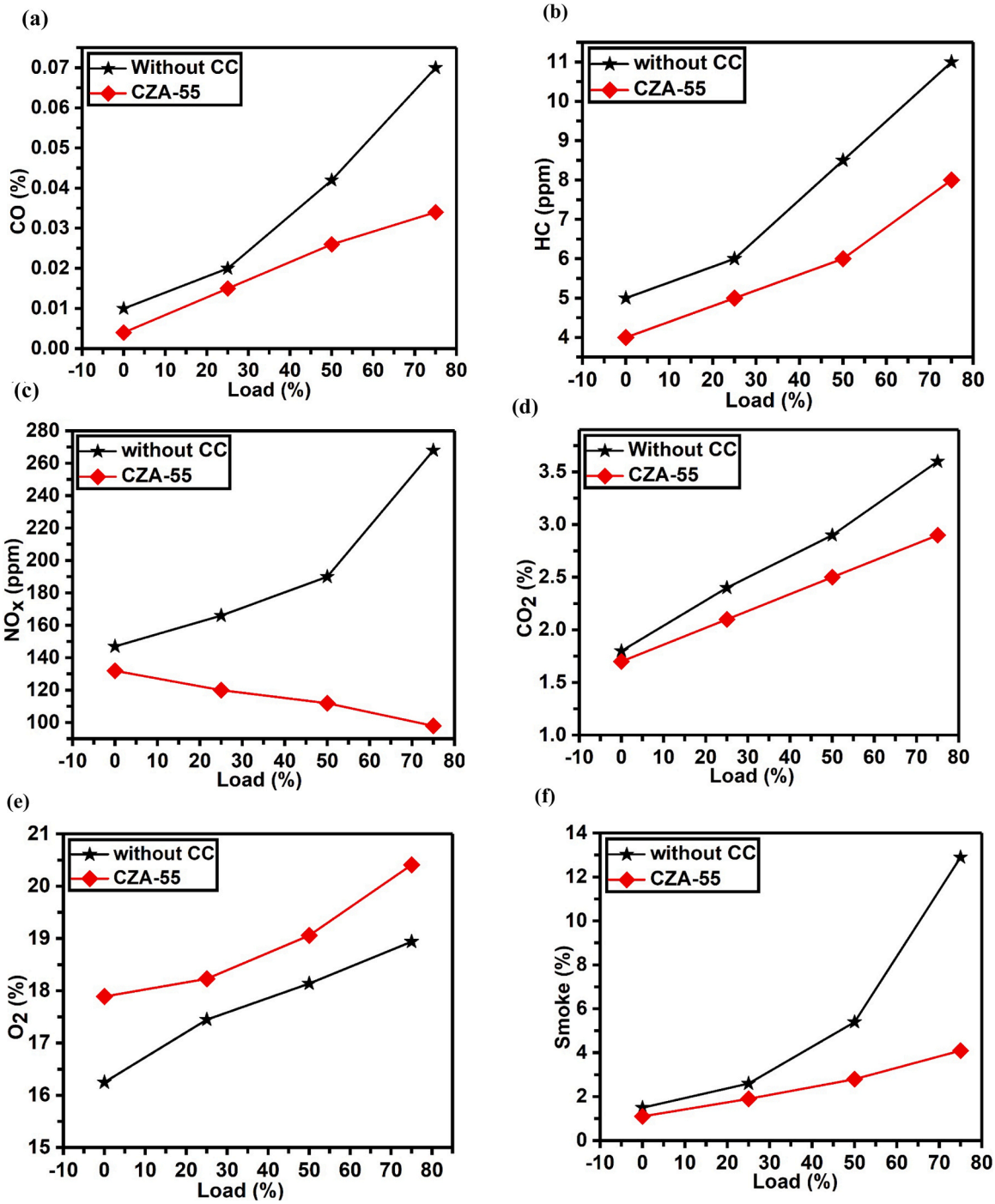

Fig. 6. Emission analysis of CZA-55 in Field Marshall diesel engine, **(a)** CO, **(b)** HC, **(c)** NO_x, **(d)** CO_2, **(e)** O_2, and **(f)** Smoke.

oxygen vacancies readily take part in the redox reactions. The oxygen spillover from the metal oxide supports to react with the soot molecules to convert them into eco-friendly gases.

4.8. *Possible reaction mechanism of CeO_2-ZrO_2/Al_2O_3 with pollutants*

In comparison to other catalysts, non-reducible ZrO_2 catalysts supported on CeO_2 and Al_2O_3 are found to be effective in oxidizing and reducing the diesel pollutants (Reddy and Khan, 2005; Di Montee and Kašpar, 2005; Atribak et al., 2010; Thammachart et al.,

2001). The observed microstructural and chemical structure properties of the CZA-55 catalyst actively participate in redox reactions by influencing the surface energy and its chemical properties. The observed unimodal pore-size distribution from BJH plot confirms congenial pore sizes, which is suitable for the chemisorption process. This proves that there is a linear correlation between the surface area of the sample and soot contact activity. The oxygen atoms on the surface and bulk bounded to the cations, which contribute to the reactants by creating and refilling the oxygen vacancies generated, known as Mars-Van-Krevelen mechanism (Dey et al., 2017).

The synergetic performance of the CeO_2-ZrO_2/Al_2O_3 sample offers an expedient pathway for reactant soot molecules to convert them into naive elements. The Ce^{4+} ions are reduced to Ce^{3+} ions with the release of oxygen vacancy. The existence of Ce^{3+} species on the surface is responsible for the CO species adhesion, which also reacts with the oxygen atoms combined with the cations (Ai et al., 2019). The CO species reacts with the lattice oxygen in Ce^{4+}-O-Zr^{4+} and produce the oxygen vacancy as Ce^{3+}-O_v-Zr^{4+} in the sample. The NO_x molecules attach on the surface of the catalyst reacts with the oxygen radicals to form their own intermediates and the final by-product N_2 dissociate from the catalyst. The surface synergetic oxygen vacancy Ce^{3+}-O_v-Zr^{4+} inflates the catalytic activity of the sample than the surface oxygen vacancy Ce^{3+}-O_v-Ce^{3+} species (Yao et al., 2014). Thus, CZA-55 sample with its appreciable redox behavior and the surface synergetic oxygen vacancy contributes substantial catalytic performance. The CZA-55 coated catalyst substrates are intended to commercialize among the industrial sectors with the help of expertise team, so the industries gain a better product in a distant future. Some recent researchers reported the emission analysis test performed using a VCR diesel engine using zirconia coated basalt fibre. The coating was made with the help of araldite and epoxy resin. The engine with neat diesel and bio-diesel blend shows less NO_x conversion in comparison with our results (Subramanian et al., 2022). Moreover, jute and Kevlar cloth were utilized as catalyst substrates with bio-diesel fuel mixture, the emission performance was tested. The emissions are quite high when compared with our CZA-55 sample (Ganesan et al., 2020, December).

5. Future aspects of the research

The present research elucidates that the noble-metal free CeO_2-ZrO_2/Al_2O_3 mixed oxides through a simple co-precipitation technique to evaluate the catalytic activity in the lean-burn diesel condition. The CZA-55 sample with higher surface area and synergistic performance of the oxygen vacancy (Ce^{3+}– Ov – Zr^{4+}) states facilitating the exhaust treatment as a better alternative to noble-metal based catalysts. However, this study is limited to short-term activity without λ-trajectory monitoring, pressure drop measurements and repeated load runs for statistical evaluation. To strengthen the practical applicability, our future studies include all the mentioned parameters along with the in-situ characterizations like O_2-TPD, and H_2-TPR studied to provide direct evidence of oxygen ion mobility for the proposed Mars-van Krevelen mechanism pathway for redox activity. These systematic approaches would strengthen the advanced CeO_2-ZrO_2/Al_2O_3 catalysts towards more qualitative, scalable and durable products for diesel exhaust treatment.

6. Conclusions

Among the three Ce/Zr ratios investigated, the CZA-55 exhibits mixed phase of cubic-tetragonal as confirmed by XRD, and Raman. The higher BET surface area of 91.2 m^2 g^{-1} was witnessed. The XPS spectra validated the existence of Ce^{3+} and oxygen vacancies generated from the non-stoichiometric nature of CeO_2 as well as the zirconia incorporation. Moreover, the synergistic performance of Ce^{3+}– Ov – Zr^{4+} plays a crucial role in oxygen mobility from the bulk to the surface and redox activity. These structural, textural, and surface-chemistry properties facilitate the catalytic treatment towards exhaust pollutants. The CZA-55 sample was evaluated under varying load conditions in Field Marshal diesel engine showed significant emission control. These findings highlight that a low-cost noble-metal free CeO_2-ZrO_2/Al_2O_3 catalysts delivered promising catalytic performance under lean-burn diesel conditions and holds potential for further technological development.

CRediT authorship contribution statement

Sambasivam Sangaraju: Writing – review & editing, Funding acquisition, Data curation, Conceptualization. **Elango Muniappan:** Writing – review & editing, Supervision, Investigation, Data curation, Conceptualization. **Mohd Shkir:** Visualization, Funding acquisition, Formal analysis. **Talat Ali:** Visualization, Resources, Formal analysis. **Jet-Chau Wen:** Resources, Formal analysis, Data curation. **Balaji Chettiannan:** Resources, Data curation. **Priyadharsini Natesan:** Methodology, Data curation, Conceptualization. **Varuna Jayachandran:** Writing – original draft, Methodology, Data curation, Conceptualization.

Declaration of Competing interest

The authors declare that they have no known competing financial interests or personal relationships that could have appeared to influence the work reported in this paper.

Acknowledgment

UAEU-AUA joint research program under grant number 12R248, and National Water and Energy Centre, United Arab Emirates University, UAE. The authors extended their appreciation to the Deanship of Research and Graduate Studies at King Khalid University for funding this work through a small Research Project under grant number RGP1/130/46.

Appendix A. Supporting information

Supplementary data associated with this article can be found in the online version at doi:10.1016/j.eti.2025.104708.

Data availability

Data will be made available on request.

References

Ai, C., Zhang, Y., Wang, P., Wang, W., 2019. Catalytic combustion of diesel soot on Ce/Zr series catalysts prepared by sol-gel method. Catalysts 9 (8), 646. https://doi.org/10.3390/catal9080646.

Anandan, C., Bera, P., 2013. XPS studies on the interaction of CeO_2 with silicon in magnetron sputtered CeO_2 thin films on Si and Si_3N_4 substrates. Appl. Surf. Sci. 283, 297–303. https://doi.org/10.1016/j.apsusc.2013.06.104.

Aneggi, E., Boaro, M., de, Leitenburg, C., Dolcetti, G., Trovarelli, A., 2006. Insights into the redox properties of ceria-based oxides and their implications in catalysis. J. Alloy. Compd. 408, 1096–1102. https://doi.org/10.1016/j.jallcom.2004.12.113.

Atribak, I., Bueno-Lopez, A., Garcia-Garcia, A., 2009. Further insights into the key features of ceria–zirconia mixed oxides governing the catalysed soot combustion under NO_x/O_2. Top. Catal. 52 (13), 2088–2091. https://doi.org/10.1007/s11244-009-9388-9.

Atribak, I., Guillén-Hurtado, N., Bueno-López, A., García-García, A., 2010. Influence of the physico-chemical properties of CeO_2–ZrO_2 mixed oxides on the catalytic oxidation of NO to NO_2. Appl. Surf. Sci. 256 (24), 7706–7712. https://doi.org/10.1016/j.apsusc.2010.06.042.

Balakrishnan, U., Tsaneva, M., 2021. Air pollution and academic performance: Evidence from India. World Dev. 146, 105553. https://doi.org/10.1016/j.worlddev.2021.105553.

Burroughs, P., Hamnett, A., Orchard, A.F., Thornton, G., 1976. Satellite structure in the X-ray photoelectron spectra of some binary and mixed oxides of lanthanum and cerium. J. Chem. Soc. Dalton Trans. (17), 1686–1698. https://doi.org/10.1039/DT9760001686.

Chen, K., Wan, J., Lin, J., Zhou, R., 2022. Comparative study of three-way catalytic performance over Pd/CeO_2-ZrO_2-Al_2O_3 and Pd/La-Al_2O_3 catalysts: new insights into microstructure and thermal stability. J. Mol. Catal. 526, 112361. https://doi.org/10.1016/j.mcat.2022.112361.

Chen, H., Ye, Z., Cui, X., Shi, J., Yan, D., 2011. A novel mesostructured alumina–ceria–zirconia tri-component nanocomposite with high thermal stability and its three-way catalysis. Micro Mesopor. Mat. 143 (2-3), 368–374. https://doi.org/10.1016/j.micromeso.2011.03.021.

Choudhary, Arti, Gokhale, Sharad, 2019. On-road measurements and modelling of vehicular emissions during traffic interruption and congestion events in an urban traffic corridor. Atmos. Pollut. Res 10 (2), 480–492. https://doi.org/10.1016/j.apr.2018.09.008.

Dai, F., Yu, Y., Meng, M., Zhang, J., Zheng, L., Hu, T., 2014. Effects of synthesis routes on the states and catalytic performance of manganese oxides used for diesel soot combustion. Catal. Lett. 144 (7), 1210–1218. https://doi.org/10.1007/s10562-014-1268-7.

Deng, Q.F., Zhang, H., Hou, X.X., Ren, T.Z., Yuan, Z.Y., 2012. High-surface-area $Ce_{0.8}Zr_{0.2}O_2$ solid solutions supported Ni catalysts for ammonia decomposition to hydrogen. Int. J. Hydrog. Energy 37 (21), 15901–15907. https://doi.org/10.1016/j.ijhydene.2012.08.069.

Dey, S., Dhal, G.C., Prasad, R., Mohan, D., 2017. Effect of nitrate metal (Ce, Cu, Mn and Co) precursors for the total oxidation of carbon monoxide. Resour. Eff. Technol. 3 (3), 293–302. https://doi.org/10.1016/j.reffit.2016.12.010.

Dey, S., Dhal, G.C., 2020. Controlling carbon monoxide emissions from automobile vehicle exhaust using copper oxide catalysts in a catalytic converter. Mater. Today Chem. 17, 100282. https://doi.org/10.1016/j.mtchem.2020.100282.

Dey, S., Mehta, N.S., 2020. Automobile pollution control using catalysis. Resour. Environ. Sustain 2, 100006. https://doi.org/10.1016/j.resenv.2020.100006.

Di Monte, R., Kašpar, J., 2005. Heterogeneous environmental catalysis–a gentle art: CeO_2–ZrO_2 mixed oxides as a case history. Catal. Today 100 (1-2), 27–35. https://doi.org/10.1016/j.cattod.2004.11.005.

Elidrissi, B., Addou, M., Regragui, M., Monty, C., Bougrine, A., Kachouane, A., 2000. Structural and optical properties of CeO_2 thin films prepared by spray pyrolysis. Thin Solid Films 379 (1-2), 23–27. https://doi.org/10.1016/S0040-6090(00)01404-8.

Enzo, S., Delogu, F., Frattini, R., Primavera, A., Trovarelli, A., 2000. Structural characterization of ceria–zirconia powder catalysts prepared by high-energy mechanical milling: a neutron diffraction study. J. Mater. Res. 15 (7), 1538–1545. https://doi.org/10.1557/JMR.2000.0220.

Feng, F., Li, H., Yang, X., Wang, C., Zhao, Y., Wang, H., Du, J., 2024. The effect P additive on the CeZrAl support properties and the activity of the pd catalysts in propane oxidation. J. Mater. 17 (5), 1003. https://doi.org/10.3390/ma17051003.

Fornasiero, P., Balducci, G., Di Monte, R., Kašpar, J., Sergo, V., Gubitosa, G., Ferrero, A., Graziani, M., 1996. Modification of the redox behaviour of CeO_2 induced by structural doping with ZrO_2. J. Catal. 164 (1), 173–183. https://doi.org/10.1006/jcat.1996.0373.

Fu, Y.P., Hu, S.H., Liu, B.L., 2009. Structure characterization and mechanical properties of CeO_2–ZrO_2 solid solution system. Ceram. Int. 35 (8), 3005–3011. https://doi.org/10.1016/j.ceramint.2009.04.001.

Fu, M., Yue, X., Ye, D., Ouyang, J., Huang, B., Wu, J., Liang, H., 2010. Soot oxidation via CuO doped CeO_2 catalysts prepared using coprecipitation and citrate acid complex-combustion synthesis. Catal. Today 153 (3-4), 125–132. https://doi.org/10.1016/j.cattod.2010.03.017.

Fuentes, R.O., Acuna, L.M., Zimicz, M.G., Lamas, D.G., Sacanell, J.G., Leyva, A.G., Baker, R.T., 2008. Formation and structural properties of Ce− Zr mixed oxide nanotubes. Chem. Mater. 20 (23), 7356–7363. https://doi.org/10.1021/cm801680c.

Galtayries, A., Sporken, R., Riga, J., Blanchard, G., Caudano, R., 1998. XPS comparative study of ceria/zirconia mixed oxides: powders and thin film characterization. J. Electron Spectrosc. Relat. Phenom. 88, 951–956. https://doi.org/10.1016/S0368-2048(97)00134-5.

Ganesan, S., Purushothaman, M., Venkatesan, S.P., Anand, K.V., Hemanandh, J., Senthilkumar and Sreenivasan, K.S., 2020, December. Experimental investigation of catalytic convertor using jute and Kevlar composite in VCR engine. In: AIP Conf. Proc, 2311. AIP Publishing LLC. https://doi.org/10.1063/5.0034014.

Guo, M., Li, H., Zhang, Y., Zhang, A., Zhao, D., Du, J., 2024. Comparative investigation of three-way conversion over palladium-based catalysts supported on phosphorus-doped and phosphorus-free ceria–zirconia–alumina. J. Phys. Chem. C. 128 (23), 9566–9577. https://doi.org/10.1021/acs.jpcc.4c02491.

Gupta, A., Waghmare, U.V., Hegde, M.S., 2010. Correlation of oxygen storage capacity and structural distortion in transition-metal-, noble-metal-, and rare-earth-ion-substituted CeO_2 from first principles calculation. Chem. Mater. 22 (18), 5184–5198. https://doi.org/10.1021/cm101145d.

Hongmei, L.I., Qingchao, Z.H.U., Yile, L.I., Maochu, G., Yongdong, C., Jianli, W., Yaoqiang, C., 2010. Effects of ceria/zirconia ratio on properties of mixed CeO_2-ZrO_2-Al_2O_3 compound. J. Rare Earths 28 (1), 79–83. https://doi.org/10.1016/S1002-0721(09)60055-7.

Jayachandran, V., Dhandapani, V.S., Muniappan, E., Park, D., Kim, B., Arun, A.P., Ayyappan, P.R., 2022. Assessment of the synergetic performance of nanostructured CeO_2-SnO_2/Al_2O_3 mixed oxides on automobile exhaust control. J. Mater. 15 (23), 8460. https://doi.org/10.3390/ma15238460.

Kanazawa, T., Suzuki, J., Takada, T., Suzuki, T., Morikawa, A., Suda, A., Sobukawa, H., Sugiura, M., 2003. 91 Development of three-way catalyst using composite alumina-ceria-zirconia. Stud. Surf. Sci. Catal. 145, 415–418. https://doi.org/10.1016/S0167-2991(03)80248-3.

Khodke, A., Watabe, A., Mehdi, N., 2021. Implementation of accelerated policy-driven sustainability transitions: case of Bharat Stage 4–6 leapfrogs in India. Sustainability 13 (8), 4339. https://doi.org/10.3390/su13084339.

Kim, J.R., Myeong, W.J., Ihm, S.K., 2009. Characteristics of CeO_2–ZrO_2 mixed oxide prepared by continuous hydrothermal synthesis in supercritical water as support of Rh catalyst for catalytic reduction of NO by CO. J. Catal. 263 (1), 123–133. https://doi.org/10.1016/j.jcat.2009.02.001.

Kozlov, A.I., Kim, D.H., Yezerets, A., Andersen, P., Kung, H.H., Kung, M.C., 2002. Effect of preparation method and redox treatment on the reducibility and structure of supported ceria–zirconia mixed oxide. J. Catal. 209 (2), 417–426. https://doi.org/10.1006/jcat.2002.3644.

Kuhn, M., Bishop, S.R., Rupp, J.L.M., Tuller, H.L., 2013. Structural characterization and oxygen nonstoichiometry of ceria-zirconia ($Ce_{1-x}Zr_xO_{2-\delta}$) solid solutions. Acta Mater. 61 (11), 4277–4288. https://doi.org/10.1016/j.actamat.2013.04.001.

Lan, L., Chen, S., Zhao, M., Gong, M., Chen, Y., 2014. The effect of synthesis method on the properties and catalytic performance of $Pd/Ce_{0.5}Zr_{0.5}O_2$-Al_2O_3 three-way catalyst. J. Mol. Catal. A Chem. 394, 10–21. https://doi.org/10.1016/j.molcata.2014.06.032.

Lee, C., Jeon, Y., Kim, T., Tou, A., Park, J.I., Einaga, H., Shul, Y.G., 2018. Ag-loaded cerium-zirconium solid solution oxide nano-fibrous webs and their catalytic activity for soot and CO oxidation. Fuel 212, 395–404. https://doi.org/10.1016/j.fuel.2017.10.007.

Letichevsky, S., Tellez, C.A., de Avillez, R.R., da Silva, M.I.P., Fraga, M.A., Appel, L.G., 2005. Obtaining CeO_2–ZrO_2 mixed oxides by coprecipitation: role of preparation conditions. Appl. Catal. B Environ. 58 (3-4), 203–210. https://doi.org/10.1016/j.apcatb.2004.10.014.

Li, J., Liu, X., Zhan, W., Guo, Y., Guo, Y., Lu, G., 2016. Preparation of high oxygen storage capacity and thermally stable ceria–zirconia solid solution. Catal. Sci. Technol. 6 (3), 897–907. https://doi.org/10.1039/C5CY01571E.

Lu, W., Iwasa, Y., Ou, Y., Jinno, D., Kamiyama, S., Petersen, P.M., Ou, H., 2017. Effective optimization of surface passivation on porous silicon carbide using atomic layer deposited Al_2O_3. RSC Adv. 7 (14), 8090–8097. https://doi.org/10.1039/C6RA27281A.

Machida, M., Kawada, T., Fujii, H., Hinokuma, S., 2015. The role of CeO_2 as a gateway for oxygen storage over CeO_2-grafted Fe_2O_3 composite materials. J. Phys. Chem. 119 (44), 24932–24941. https://doi.org/10.1021/acs.jpcc.5b09876.

Monte, R.D., Kašpar, J., 2004. On the role of oxygen storage in three-way catalysis. Top. Catal. 28 (1), 47–57. https://doi.org/10.1023/B:TOCA.0000024333.08447.f7.

Mullins, D.R., Overbury, S.H., Huntley, D.R., 1998. Electron spectroscopy of single crystal and polycrystalline cerium oxide surfaces. Surf. Sci. 409 (2), 307–319. https://doi.org/10.1016/S0039-6028(98)00257-X.

Myung, J.H., Shin, T.H., Huang, X., Carins, G., Irvine, J.T., 2015. Enhancement of redox stability and electrical conductivity by doping various metals on ceria, $Ce_{1-x}M_xO_{2-\delta}$ (M= Ni, Cu, Co, Mn, Ti, Zr). Int. J. Hydrog. Energy 40 (35), 12003–12008. https://doi.org/10.1016/j.ijhydene.2015.05.029.

Pandey, A., Brauer, M., Cropper, M.L., Balakrishnan, K., Mathur, P., Dey, S., Turkgulu, B., Kumar, G.A., Khare, M., Beig, G., Gupta, T., 2021. Health and economic impact of air pollution in the states of India: the Global Burden of Disease Study 2019. Lancet Planet Health 5 (1), e25–e38. https://doi.org/10.1016/S2542-5196(20)30298-9.

Papavasiliou, A., Tsetsekou, A., Matsouka, V., Konsolakis, M., Yentekakis, I.V., Boukos, N., 2009. Development of a Ce–Zr–La modified Pt/γ-Al_2O_3 TWCs' washcoat: effect of synthesis procedure on catalytic behaviour and thermal durability. Appl. Catal. B Environ. 90 (1-2), 162–174. https://doi.org/10.1016/j.apcatb.2009.03.006.

Petkovich, N.D., Rudisill, S.G., Venstrom, L.J., Boman, D.B., Davidson, J.H., Stein, A., 2011. Control of heterogeneity in nanostructured Ce_1_xzr$_xO_2$ binary oxides for enhanced thermal stability and water splitting activity. J. Phys. Chem. C. 115 (43), 21022–21033. https://doi.org/10.1021/jp2071315.

Piumetti, M., Bensaid, S., Fino, D., Russo, N., 2016. Nanostructured ceria-zirconia catalysts for CO oxidation: study on surface properties and reactivity. Appl. Catal. B Environ. 197, 35–46. https://doi.org/10.1016/j.apcatb.2016.02.023.

Reddy, B.M., Khan, A., 2005. Nanosized CeO_2–SiO_2, CeO_2–TiO_2, and CeO_2–ZrO_2 mixed oxides: influence of supporting oxide on thermal stability and oxygen storage properties of ceria. Catal. Surv. Asia 9 (3), 155–171. https://doi.org/10.1007/s10563-005-7552-1.

Ren, Z., Wang, P., Kong, J., Wang, M., Chang, L., 2017. Structures and oxygen storage/release capacities of $Ce_xZr_{1-x}O_2$: effects of Zr content and preparation method. J. Energy Chem. 26 (4), 647–654. https://doi.org/10.1016/j.jechem.2017.04.003.

Rossignol, S., Gérard, F., Duprez, D., 1999b. Effect of the preparation method on the properties of zirconia-ceria materials. J. Mater. Chem. 9 (7), 1615–1620. https://doi.org/10.1039/A900536F.

Rossignol, S., Madier, Y., Duprez, D., 1999a. Preparation of zirconia–ceria materials by soft chemistry. Catal. Today 50 (2), 261–270. https://doi.org/10.1016/S0920-5861(98)00508-2.

Ruppi, S., Larsson, A., Flink, A., 2008. Nanoindentation hardness, texture and microstructure of α-Al_2O_3 and κ-Al_2O_3 coatings. Thin Solid Films 516 (18), 5959–5966. https://doi.org/10.1016/j.tsf.2007.10.078.

Sellick, D.R., Aranda, A., García, T., López, J.M., Solsona, B., Mastral, A.M., Morgan, D.J., Carley, A.F., Taylor, S.H., 2013. Influence of the preparation method on the activity of ceria zirconia mixed oxides for naphthalene total oxidation. Appl. Catal. B Environ. 132, 98–106. https://doi.org/10.1016/j.apcatb.2012.11.036.

Subramanian, L.S., Ganesan, S., Venkatesan, S.P., Muniappan, P., Pugazhenthi, R., 2022. Experimental analysis of VCR diesel engine exhaust emissions with zirconium dioxide and basalt based catalytic converter using lemon grass oil. Mater. Today Proc. 60, 1949–1958. https://doi.org/10.1016/j.matpr.2022.01.143.

Terribile, D., Trovarelli, A., Llorca, J., de Leitenburg, C., Dolcetti, G., 1998. The preparation of high surface area CeO_2–ZrO_2 mixed oxides by a surfactant-assisted approach. Catal. Today 43 (1-2), 79–88. https://doi.org/10.1016/S0920-5861(98)00136-9.

Thammachart, M., Meeyoo, V., Risksomboon, T., Osuwan, S., 2001. Catalytic activity of CeO_2–ZrO_2 mixed oxide catalysts prepared via sol–gel technique: CO oxidation. Catal. Today 68 (1-3), 53–61. https://doi.org/10.1016/S0920-5861(01)00322-4.

Venkataswamy, P., Jampaiah, D., Rao, K.N., Reddy, B.M., 2014. Nanostructured $Ce_{0.7}Mn_{0.3}O_{2-\delta}$ and $Ce_{0.7}Fe_{0.3}O_{2-\delta}$ solid solutions for diesel soot oxidation. Appl. Catal. A Gen. 488, 1–10. https://doi.org/10.1016/j.apcata.2014.09.014.

Vojtko, M., Puchy, V., Múdra, E., Milkovič, O., Kovalčíková, A., 2020. Coarse-grain CeO_2 doped ZrO_2 ceramic prepared by spark plasma sintering. J. Eur. Ceram. Soc. 40 (14), 4844–4852. https://doi.org/10.1016/j.jeurceramsoc.2020.05.014.

Wan, Q., Duan, L., He, K., Li, J., 2011. Removal of gaseous elemental mercury over a CeO_2–WO_3/TiO_2 nanocomposite in simulated coal-fired flue gas. Chem. Eng. J. 170 (2-3), 512–517. https://doi.org/10.1016/j.cej.2010.11.060.

Wei, Z., Li, H., Zhang, X., Yan, S., Lv, Z., Chen, Y., Gong, M., 2008. Preparation and property investigation of CeO_2–ZrO_2–Al_2O_3 oxygen-storage compounds. J. Alloy. Compd. 455 (1-2), 322–326. https://doi.org/10.1016/j.jallcom.2007.01.060.

Wu, D., Zhang, H., 2013. Mechanical stability of monolithic catalysts: scattering of washcoat adhesion and failure mechanism of active material. Ind. Eng. Chem. Res. 52 (41), 14713–14721. https://doi.org/10.1021/ie402546q.

Yang, L., Lin, S., Yang, X., Fang, W., Zhou, R., 2014. Promoting effect of alkaline earth metal doping on catalytic activity of HC and NO_x conversion over Pd-only three-way catalyst. J. Hazard. Mater. 279, 226–235. https://doi.org/10.1016/j.jhazmat.2014.06.076.

Yao, X., Xiong, Y., Zou, W., Zhang, L., Wu, S., Dong, X., Gao, F., Deng, Y., Tang, C., Chen, Z., Dong, L., 2014. Correlation between the physicochemical properties and catalytic performances of $Ce_xSn_{1-x}O_2$ mixed oxides for NO reduction by CO. Appl. Catal. B Environ. 144, 152–165. https://doi.org/10.1016/j.apcatb.2013.06.020.

Yashima, M., Sasaki, S., Yamaguchi, Y., Kakihana, M., Yoshimura, M., Mori, T., 1998. Internal distortion in ZrO_2–CeO_2 solid solutions: neutron and high-resolution synchrotron x-ray diffraction study. Appl. Phys. Lett. 72 (2), 182–184. https://doi.org/10.1063/1.120678.

Yu, G., Zhu, L., Zhang, G., Qin, G., Fu, H., Ji, F., Zhao, J., 2014. Preparation and characterization of the continuous titanium-doped ZrO_2 mesoporous fibers with large surface area. J. Porous Mater. 21 (1), 105–112. https://doi.org/10.1007/s10934-013-9753-8.

Zhang, F., Chen, C.H., Hanson, J.C., Robinson, R.D., Herman, I.P., Chan, S.W., 2006. Phases in ceria–zirconia binary oxide $_{(1-x)}CeO_{2-x}ZrO_2$ nanoparticles: the effect of particle size. J. Am. Ceram. Soc. 89 (3), 1028–1036. https://doi.org/10.1111/j.1551-2916.2005.00788.x.

Zhao, S., Kang, D., Liu, Y., Wen, Y., Xie, X., Yi, H., Tang, X., 2020. Spontaneous formation of asymmetric oxygen vacancies in transition-metal-doped CeO_2 nanorods with improved activity for carbonyl sulfide hydrolysis. ACS Catal. 10 (20), 11739–11750. https://doi.org/10.1021/acscatal.0c02832.

Zhao, B., Li, G., Ge, C., Wang, Q., Zhou, R., 2010. Preparation of $Ce_{0.67}Zr_{0.33}O_2$ mixed oxides as supports of improved Pd-only three-way catalysts. Appl. Catal. B Environ. 96 (3-4), 338–349. https://doi.org/10.1016/j.apcatb.2010.02.031.

Zhou, C., Zhang, H., Zhang, Z., Li, L., 2021. Improved reactivity for toluene oxidation on MnO_x/CeO_2-ZrO_2 catalyst by the synthesis of cubic-tetragonal interfaces. Appl. Surf. Sci. 539, 148188. https://doi.org/10.1016/j.apsusc.2020.148188.